Title

The effects of bathymetry on the long-term carbon cycle and CCD.

Journal

Proceedings of the National Academy of Sciences, 121(21)

Authors

Bogumil, Matthew
Mittal, Tushar
Lithgow-Bertelloni, Carolina

Publication Date

2024-05-21

DOI

10.1073/pnas.2400232121

Peer reviewed

PNAS RESEARCH ARTICLE | EARTH, ATMOSPHERIC, AND PLANETARY SCIENCES

The effects of bathymetry on the long-term carbon cycle and CCD

Matthew Bogumil[a,1], Tushar Mittal[b], and Carolina Lithgow-Bertelloni[a]

Edited by Donald Canfield, Syddansk Universitet, Odense M., Denmark; received January 5, 2024; accepted April 3, 2024

The shape of the ocean floor (bathymetry) and the overlaying sediments provide the largest carbon sink throughout Earth's history, supporting ~one to two orders of magnitude more carbon storage than the oceans and atmosphere combined. While accumulation and erosion of these sediments are bathymetry dependent (e.g., due to pressure, temperature, salinity, ion concentration, and available productivity), no systemic study has quantified how global and basin scale bathymetry, controlled by the evolution of tectonics and mantle convection, affects the long-term carbon cycle. We reconstruct bathymetry spanning the last 80 Myr to describe steady-state changes in ocean chemistry within the Earth system model LOSCAR. We find that both bathymetry reconstructions and representative synthetic tests show that ocean alkalinity, calcite saturation state, and the carbonate compensation depth (CCD) are strongly dependent on changes in shallow bathymetry (ocean floor ≤600 m) and on the distribution of the deep marine regions (>1,000 m). Limiting Cenozoic evolution to bathymetry alone leads to predicted CCD variations spanning 500 m, 33 to 50% of the total observed variations in the paleoproxy records. Our results suggest that neglecting bathymetric changes leads to significant misattribution to uncertain carbon cycle parameters (e.g., atmospheric CO_2 and water column temperature) and processes (e.g., biological pump efficiency and silicate-carbonate riverine flux). To illustrate this point, we use our updated bathymetry for an Early Paleogene C cycle case study. We obtain carbonate riverine flux estimates that suggest a reversal of the weathering trend with respect to present-day, contrasting with previous studies, but consistent with proxy records and tectonic reconstructions.

long-term carbon cycle | bathymetry | planetary feedbacks

Significance

Our study illustrates that seafloor bathymetry—both mean depth as well as bathymetry distribution—has a significant influence on the global carbon cycle by controlling the location of seafloor carbonate sedimentation. Considering the plausible range of bathymetric configurations over the last 80 Myr of Earth's history, bathymetry cannot be ignored when studying the carbon cycle and inferring changes in ocean chemistry and productivity.

The long-term surface carbon cycle is a balance of carbon fluxes between sources (e.g., volcanic emissions) and sinks (carbon burial by carbonate-bearing minerals and organic-rich sediments on the seafloor, which are then recycled via subduction). Silicate weathering on land or seafloor is a source of a) bicarbonate ions, acting as a short-term carbon sink through the removal of atmospheric carbon and b) cations (Ca^{2+}, Mg^{2+}, $Fe^{2,3+}$, Eq. **1**). These are physically transported to ocean basins by rivers and eventually deposited in ocean sediments. Thus, weathering generates ocean alkalinity, which leads to long-term carbon removal from the ocean–atmosphere system. On timescales of 10 s of Myr, studies suggest that the carbon cycle reaches a steady state, wherein the ocean bicarbonate concentration is largely modulated by dissolved continental rocks (Eq. **1**) and dissolution of atmospheric CO_2 into the ocean's surface (Eq. **2**). However, this is an end-member perspective focused on carbon (C) sources and sinks without detailed consideration of *how* the steady state is achieved. Instead, it implicitly assumes that ocean chemistry and carbonate deposition always adapt to reach the required C sink to match the C sources. Most studies of long-term carbon cycle dynamics for Earth and other planetary bodies make these assumptions.

Silicate weathering:

$$CaSiO_3 + 2CO_{2(aq)} + H_2O \rightarrow Ca^{2+} + 2HCO_3^- + SiO_2. \quad [1]$$

Ocean carbonate chemistry:

$$CO_{2(atm)} \rightleftharpoons CO_{2(aq)} + H_2O_{(l)} \rightleftharpoons H^+ + HCO_3^- \rightleftharpoons CO_3^{2-} + 2H^+. \quad [2]$$

Carbonate precipitation:

$$Ca^{2+} + 2HCO_3^- \rightleftharpoons CaCO_3 + CO_{2(aq)} + H_2O. \quad [3]$$

A different perspective for the C cycle focuses on the dynamics of marine carbonate precipitation, dissolution, and deposition: the net rate of carbonate deposition determines the evolution toward steady state. This perspective highlights the important role of the ocean as the dominant surface C reservoir as well as the main buffer for short-term C cycle

Author affiliations: [a]Department of Earth, Planetary, and Space Sciences, University of California, Los Angeles, CA 90095-1567; and [b]Department of Geosciences, The Pennsylvania State University, University Park, PA 16802

Author contributions: M.B., T.M., and C.L.-B. designed research; M.B., T.M., and C.L.-B. performed research; M.B., T.M., and C.L.-B. analyzed data; M.B. developed models/codes.; T.M. and C.L.-B. contributed to writing and editing of manuscript; and M.B. wrote the paper.

The authors declare no competing interest.

This article is a PNAS Direct Submission.

[1]To whom correspondence may be addressed. Email: matthewbogumil@ucla.edu.

This article contains supporting information online at https://www.pnas.org/lookup/suppl/doi:10.1073/pnas.2400232121/-/DCSupplemental.

Published May 15, 2024.

perturbations, due to the high solubility of CO_2 in water (1). Marine carbonate chemistry (Eq. **2**) allows the ocean to take up far more CO_2 than expected based on CO_2 solubility alone, by transforming added CO_2 into HCO_3^- and CO_3^{2-} ions [together termed dissolved inorganic carbon (DIC)]. The dissolved carbonate ions in seawater are eventually biotically and abiotically precipitated as carbonate-bearing minerals (calcite, aragonite, magnesite, and siderite) through ocean productivity, primarily in surface waters (Eq. **3**, long-term C sink). After precipitation, $CaCO_3$ particles sink to the deeper ocean via the biological pump, where they are either deposited or dissolved. Dissolution of $CaCO_3$ (calcite and aragonite) in the deep ocean is driven by increasing solubility with increasing pressure and decreasing temperature (2). The lysocline marks the depth interval in the ocean where ~90% $CaCO_3$ dissolves, while the carbonate compensation depth (CCD) is the depth below which all newly formed $CaCO_3$ is dissolved. However, the exact depths (pressure) of the lysocline and CCD in an ocean basin are dependent on its seawater chemistry: primarily the DIC and alkalinity. In a deposition/precipitation focused perspective of the C cycle, the depth and the spatial distribution of the seafloor depositional area (i.e., the seafloor bathymetry) directly determines the area of seafloor above the lysocline and consequently the carbonate burial efficiency. This, in turn, controls seafloor carbonate coverage, ocean carbonate chemistry, and hence atmospheric CO_2 concentration, as well as the ocean's ability to buffer any fast and large CO_2 releases from volcanic eruptions.

Therefore, we expect bathymetry to strongly influence the net rate of ocean C burial and the carbonate saturation in the oceans as it adjusts to reach the long-term steady state. In this study, we highlight the critical role of seafloor bathymetry on the evolution of the marine C cycle, using idealized marine carbonate cycle models that modulate the available shallow (≤600 m) vs deep (>1,000 m) ocean floor area. Because the mean depth and relative depth distribution of the seafloor is directly controlled by the speed of plate tectonics, mantle flow, and relative sea level, our results highlight a hitherto unappreciated strong coupling between planetary interiors and surface climate through chemical processes. This coupling is important because it evolves significantly through time as ocean basin structure changes in response to large-scale tectonic and convective processes, such as super-continent formation and breakup (3, 4). For instance, as plate motions slowed throughout the last 100 Myr, more thermal subsidence has deepened ocean basins (Fig. 1) (5, 6).

Our study focuses explicitly on the chemical effects of bathymetry on Earth's ocean–atmosphere system. This is distinct and complementary to the effect of bathymetry on the physical dynamics of the ocean through changes in ocean circulation, mixing, and heat flux. For instance, ocean circulation is strongly influenced by the opening and closing of ocean basins (e.g., closure of the Tethys and opening of the Atlantic) and the development of gateways between them (e.g., Drake's Passage, Tasman opening, and closure of the Central American Seaway, e.g., refs. 7–9). Both global circulation and vertical mixing rates (also sensitive to seafloor bathymetry) contribute to varied regional/global water column ocean chemistry and nutrient availability (10). However, these studies do not analyze the effects of changing bathymetry on ocean carbonate deposition/dissolution.

The limited work on the chemical effects of bathymetric changes has focused on using bathymetry as a boundary condition to determine solid earth carbon fluxes, the impact of continental shelf evolution on biotic productivity, or the evolution of continental shelves on the long-term carbon cycle. For instance, atmospheric CO_2 concentrations were found to have been impacted by shallow carbonate burial during the Quaternary large glacial-interglacial sea-level changes (11, 12). On timescales of 1 to 10 s of Myr, Komar and Zeebe proposed that changes in ocean chemistry, previously attributed to long-term global carbonate weathering trends, could instead be linked to shelf productivity evolution coinciding with continental flooding (13). Mesozoic–Cenozoic sedimentary carbon subduction and degassing fluxes have been computed using depositional zones, defined by the intersection of a reconstructed CCD with evolving bathymetry (14, 15). While these previous studies highlight integral roles of the bathymetric effect on the carbon cycle, bathymetry itself is not integrated into the C cycle dynamics. Instead, they focus on bathymetry as a carbon transport facilitator. They do not explore how bathymetry influences when, where, and how much carbon-bearing sediment is deposited or distinguish between the role of mean depth vs. bathymetric distribution.

Here, we address this critical knowledge gap. We utilize a commonly implemented intermediate complexity Earth system model—Long-term Ocean-Sediment-CArbon cycle Reservoir (LOSCAR) (*SI Appendix*. Fig. S1) that allows for the analysis of basin-scale ocean chemical responses in the water column and seafloor sediments (16). The Earth system is spatially resolved to first order—laterally with different ocean basin boxes to simplify dynamics, and vertically to represent depositional surfaces. We use LOSCAR for this study, instead of more complex Earth system models such as CGenie (17) because of ease of interpretation and modification. With LOSCAR, we can easily tease apart causation, by independently focusing on the chemical response of the ocean separately from the physical.

To gain mechanistic insights into the carbon cycle's relevant feedbacks, we first explore the cycle's sensitivity to idealized bathymetric models that use present-day basin sizes but synthetic bathymetry distributions. We then create and use a unique reconstruction of global bathymetry for the last 80 Myr (in 5 Ma increments) to put our results in the context of Earth's evolution. This reconstruction is based on recent ocean lithosphere age reconstructions paired with a lithospheric cooling relationship (4, 18). We account for the effect of oceanic plateaus and other intermediate depth bathymetry and eustatic sea-level changes (c.f. *Materials and Methods*). Finally, we illustrate the dramatic effect of selecting accurate seafloor bathymetry for inferring riverine flux, using the late Paleocene as a case study.

Results

Synthetic Bathymetry. We constructed synthetic bathymetry with changes in the total area of the shallow ocean within the range of estimates for the last 80 Myr (96 and 120% of present-day area, Fig. 2*D*) and changes in the average depth of deep bathymetry. For deep bathymetry, we used Gaussian distributions centered between 3.5 and 4.5 km depths (Fig. 2*D*). We use our synthetic bathymetry models directly in LOSCAR's modern three ocean system (*SI Appendix*, Fig. S1) to calculate ocean and atmosphere steady states. We keep surface weathering and alkalinity fluxes constant as we change bathymetry. To track changes in ocean chemistry, we analyze variations in the CCD and first-order (>99%, ref. 19) ocean total alkalinity ($TA = HCO_3^- + 2CO_3^{2-} B(OH)_4^- + HS^- + 2S^{2-} + OH^- - H^+ - 2SO_4^{2-}$). In our work, changes in TA are primarily driven by carbonate chemistry ($HCO_3^- + 2CO_3^{2-}$). TA measures the charge difference between the ocean's major conservative cations and anions (e.g., Cl and sulfate) and is a metric for the ocean's ability to precipitate carbonate and buffer against pH variations. From here on out TA and alkalinity are used interchangeably. Changes in ocean alkalinity are good proxies for the carbonate saturation state of the ocean.

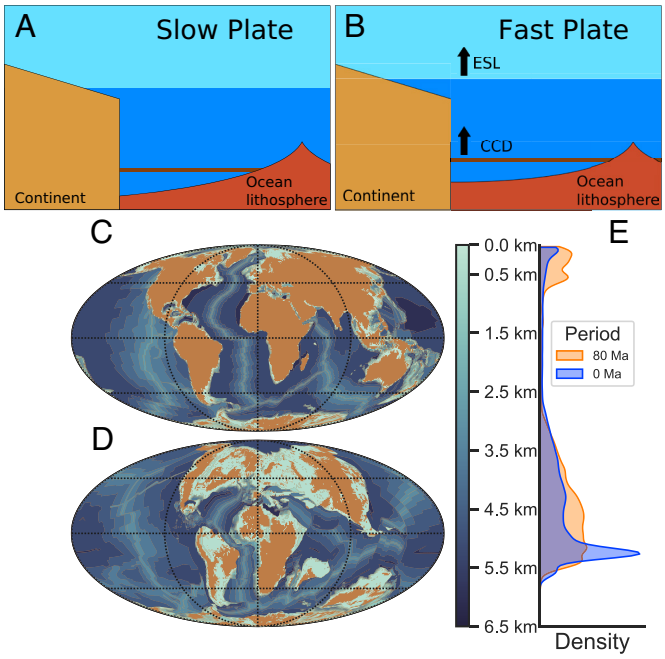

Fig. 1. Evolution of 1st and 2nd order bathymetry. (*A* and *B*) Cartoon of seafloor morphology. Deep ocean bathymetry is represented by the oceanic lithosphere (rust red), while shallow bathymetry is represented by the continent (yellow) water interface. The brown line denotes the CCD, below which no carbon is sequestered. The light and dark blue interfaces represent eustatic sea-level (ESL). These cartoons show how slow and fast plate motions lead to increased or decreased thermal subsidence, respectively, before subduction, resulting in 1st order changes in ocean floor depth, sea-level, and the CCD. Bathymetry reconstructions at present-day (*C*) and 80 Ma (*D*) represent slow (*C*) and fast plate (*D*) motion regimes. (*E*) Kernel depth distributions for (*C* and *D*) denote two major components of bathymetry evolution: 1) changes to shallow seafloor (≤600 m) area and 2) changes to the distribution and mean deep bathymetry (>1,000 m).

For example, a higher ocean TA is required to prevent dissolution and deposit carbonate in the deep ocean as opposed to shallow water continental shelves. CCD variations represent 1) changes to the depositional area in carbonate-saturated waters and 2) solid carbonate dissolution or deposition above the CCD. The CCD is a useful marine C cycle proxy because it can be observationally inferred over recent Earth history. Throughout the Cenozoic, the CCD varied between ~4.5 and 3 km depth, with perturbations marked by CO_2 forcing events (20).

First, we isolated the effects of changing the average depth of the deep ocean by choosing a constant shallow ocean area for the present-day (~30×10^6 km^2, black point in Fig. 2*A*). We find that shallowing the average deep marine depth by 500 m decreases the CCD by ~500 m (Fig. 2*A*). Physically, this can be understood as follows: as the depth of the deep ocean decreases (Fig. 2*D*), there is a reduction in the pressure-dependent calcite solubility that supports increased calcite burial rates, leading to a reduction in shallow and deep ocean alkalinity (*SI Appendix*, Fig. S3) and saturation state (*SI Appendix*, Fig. S4) when burial equilibrates with riverine alkalinity input. This leads to a drop in ocean CO_2 storage capacity, increased atmospheric CO_2, and a shoaled CCD (*SI Appendix*, Fig. S15).

Second, we isolated the effects of changing shelf bathymetry given a constant average deep bathymetry similar to present-day (4 km). Doubling the present-day shelf area (~60×10^6 km^2) leads to the CCD being shoaled by ~250 m (Fig. 2*A*). Physically, this can be understood as follows: Given constant global productivity, increased shelf area leads to increased proportion of calcite rain and burial on the shelf and decreased open ocean rain. The change in rain partitioning reduces the flux of bicarbonate to the deep ocean, decreasing the deep marine alkalinity (*SI Appendix*, Fig. S3) and calcite saturation (*SI Appendix*, Fig. S4), leading to increased deep marine dissolution and a shoaled CCD. This process is analogous to what has been proposed for Quaternary glacial changes in sea-level and the marine C cycle (coral reef hypothesis, ref. 21).

In contrast to changing mean deep ocean depths, we see two CCD shoaling trends with increasing shallow seafloor area, both stemming from shelf vs. open ocean productivity partitioning and consequent changes in carbonate burial vs dissolution. The initially weaker effect on the CCD, most evident in the Atlantic, is a result of stripping away more and more calcite deposition from the deep Pacific and Indian ocean basins as shelf area increases. This leads to large amounts of alkalinity being supplied to the shelf through deep marine calcite erosion before the earth system model reaches a steady state. However, the stronger effect (kinks at shallow area >50×10^6 km^2) appears once the Pacific and Indian oceans transition from a weak-deposition to a non-deposition regime since the CCD is above any available seafloor (*SI Appendix*, Fig. S5). Open ocean calcite rain is not deposited at all in the deep Indian and Pacific regions and significant changes in Atlantic Ocean alkalinity (and hence CCD) are needed to reach equilibrium (*SI Appendix*, Fig. S3). Subsequently, increased shelf area leads to stripping away alkalinity from the deep marine water column in the Atlantic, causing rapid decreases in the CCD. We note that the exact location of the regime transition (kink) depends on the assumed modern ocean chemistry and interbasin differences. Presently, the Atlantic Ocean has high

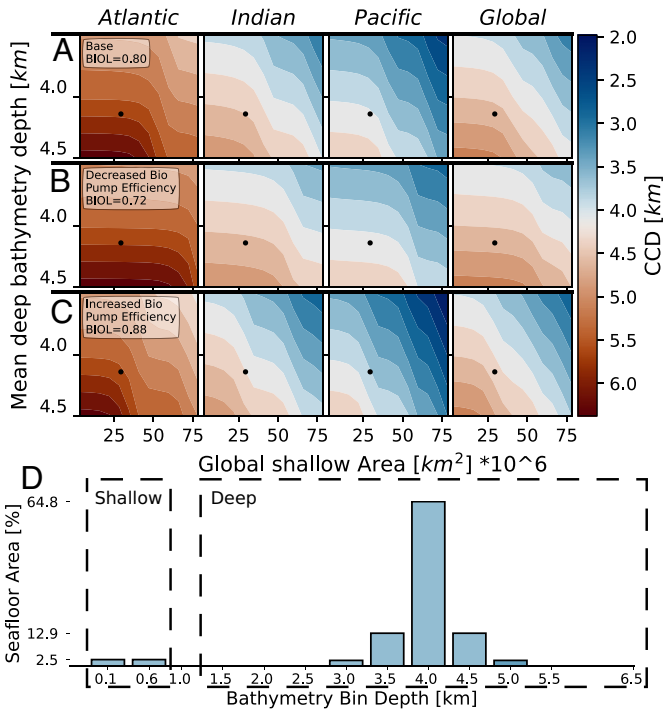

Fig. 2. Response of CCD given synthetic bathymetric distributions representing 1st order changes in deep bathymetry and shallow seafloor area. (*A*–*C*) LOSCAR bathymetry inputs shown in (*D*): 1) deep bathymetry represented through Gaussian distributions, and 2) shallow bathymetry areal extent ranging from 96 to 120% of its present value. Synthetics produce similar areal extents and average deep marine depths to those within the last 80 Myr. (*A*–*C*) columns and rows show different ocean basins and Earth system model setup, respectively. (*A*) Base model for the steady-state CCD (contours) obtained with LOSCAR modified to include our preferred bathymetry. No silicate/carbonate weathering feedback included. (*B* and *C*) Models with decreased and increased biological pump efficiency, respectively. Decreased biological pump efficiency reduces calcite rain, shallow sequestered alkalinity, and calcite erosion in the deep marine. It allows the Pacific and Indian basins to persist as depositional basins for greater shallow shelf areas.

alkalinity and a deeper CCD due to the pattern of precipitation, river influx, and ocean circulation. However, during Earth history, there is no reason to expect a priori that each ocean basin would have very similar alkalinity. We expect instead a transition in the shallow shelf CCD shoaling trend between the two end-members described above at different shallow shelf areas and mean deep ocean depths.

Overall, we find that the CCD (as a proxy for the ocean carbonate system) is strongly sensitive to bathymetry—both the global bathymetry distribution (shallow area as well as deep ocean depth) as well as the distribution within different ocean basins. However, the final extent of sensitivity will be dependent on coupled bio-geochemical-ocean dynamics processes that are not fully included. For example, while increased seafloor area led to increased shelf vs. open ocean productivity, nutrients (PO_4) upwelled from the deep ocean could become restricted and mitigate shelf productivity growth. One way to parameterize this effect on the Earth system is by decreasing the efficiency of the biological pump. Reducing the pump's efficiency by 10% with respect to the base model results in less surface water alkalinity being sequestered in the shelf area (Fig. 2*B*). Ultimately, this reduces deep ocean dissolution, allowing for calcite burial in the Pacific and Indian ocean basins, making the CCD less sensitive to changes in shelf area. On the other hand, increases in the biological pump efficiency produce the opposite effect (Fig. 2*C*). We find that our results remain essentially the same even when we include the atmospheric CO_2-dependent weathering feedback. This feedback relaxes the atmospheric CO_2 back to the initial state but not the ocean alkalinity and CCD (*SI Appendix*, Fig. S15). We find that bathymetry alone can lead to as much as 2.5 km CCD variations both within basins and globally, with accompanying shifts in calcite saturation, alkalinity, and ocean and atmospheric CO_2 (Fig. 2 and *SI Appendix*, Figs. S3 and S4).

Reconstructed Bathymetry. One of the limitations of the synthetic results is that they don't provide a direct assessment of how CCDs will change with realistic bathymetry evolution over the Cenozoic, which saw changes in the areal extent and depth distribution of individual basins due to the growth and decay of oceans. To mitigate this limitation and directly compare with Pacific & global CCD inferences, we generated unique bathymetry reconstructions, corrected for basin volume (c.f. *Materials and Methods* and *SI Appendix*, Fig. S12) over the last 80 Myr. We find significant bathymetric evolution over this time, culminating in a reduction to ~33% of the shallow ocean area at present-day with respect to 80 Ma. In addition, the average depth of the oceans deepened by ~500 m (Fig. 1). We find two primary reasons for this behavior: a) changes to shallow bathymetry (≤600 m) associated with continental topography and flooding, and changes in eustatic and relative sea-level reconstructions since the Cretaceous; b) changes in deep bathymetry (>1 km depths) occur between mid-ocean ridge depths (~2.5 km) and abyssal plain depths (~5 km) and are largely a consequence of the disappearance of the Tethys and older global seafloor compared to over the last ~80 Myr. These factors combine to generate a narrow and strongly peaked deep seafloor distribution today.

In addition to global changes, we find relative differences in the Atlantic, Indian, and Pacific Ocean basin surface areas over time (c.f. *Materials and Methods* for details regarding basin separation, *SI Appendix*, Figs. S14 and S17). Today, pelagic carbonate accumulation varies by ocean basin and is highest in the Atlantic Ocean due to the nature of ocean circulation and weathering fluxes (22, 23). Interocean basin changes hence add to the bathymetric controls on the carbon cycle. Our synthetic results (Fig. 2) demonstrate the importance of basinal bathymetric distributions through the CCD and the seafloor carbonate distribution above it (*SI Appendix*, Fig. S16).

Using our bathymetry reconstructions, we modified the bathymetry distribution in the LOSCAR present-day model setup while keeping the other ocean (e.g., mixing), atmosphere (e.g., pCO_2), global productivity, and weathering components constant at present-day values. Similar to synthetic tests, the CCDs calculated from actual bathymetry evolution deepened over the last 80 Myr with an increased average depth of deep marine seafloor and decreased shallow seafloor area. Notably, CCD variations calculated from the last 80 Myr of bathymetry evolution can describe ~33 to 50% (~500 m) of the total Cenozoic variation derived from seafloor sediment cores (Fig. 3 *B* and *D*) (20, 24). The CCD has a significant dependence on the evolution of deep bathymetry, which is tied to plate tectonics and mantle dynamics. The current lack of bathymetric representation in many C cycle models leads to a misunderstanding of the contribution of uncertain carbon cycle parameters (e.g., atmospheric CO_2, water column temperature, carbonate-silicate weathering, productivity) over 10 s of Myr. We readily acknowledge that we have simplified the processes at play, since other C cycle parameters (e.g., volcanic outgassing, pCO_2, carbonate weathering, ocean Ca^{2+} and Mg^{2+} concentrations) are also changing during this time period. However, although a full model inversion and sensitivity analysis is beyond the scope of the present study, it is clear from the magnitude of the effect that neglecting well-known changes to the shape of the marine container imperils interpretation.

Early Paleogene Case Study. As a specific example, we use Early Paleogene (pre-Paleocene-Eocene Thermal Maximum, or PETM) as a case study. This is an extensively studied and well-constrained period with a large wealth of ocean paleoclimate data (ref. 16, and references therein). We used LOSCAR's paleo

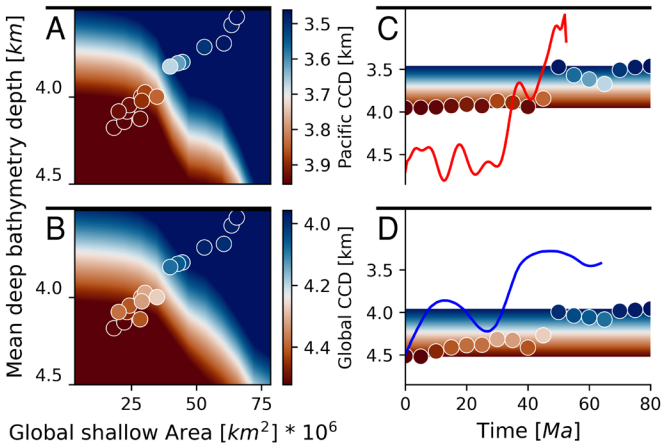

Fig. 3. Response of CCD given reconstructed bathymetry. Contours in (*A* and *B*) show the CCD for synthetic bathymetry models and dots show realistic reconstructions over the last 80 Myr for the Pacific and global ocean(s), respectively. Synthetic bathymetry modeled CCDs are plotted within reconstruction ranges. The saturation within the synthetic models indicates that CCDs calculated from realistic bathymetry reconstructions are subdued, but still lead to ~500 m variations which are exclusively bathymetric dependent. CCD evolution for the Pacific (*C*) and globally (*D*). We show (*C* and *D*) the total synthetic range shown throughout the reconstruction period. The blue and red curves represent the Lyle et al. (24) global CCD and Palike et al. (20) equatorial CCD, respectively. Notably, reconstructions show the CCD shoaling between 65 to 50 Ma and deepening between 30 Ma and present-day. The major CCD deepening between 50 and 40 Ma occurred concurrently with bathymetric changes resulting from the India-Asia collision.

setup which represents conditions before the PETM, including paleobathymetry for the four major ocean basins (Fig. 4*A*). First, we updated the bathymetry model with our 60 Ma reconstruction (Fig. 4*A*) and reduced the shelf vs open ocean production partitioning factor by 50% (to numerically stabilize the model). In steady-state, the C system responded to updated bathymetry by deepening the global CCD by ~2 km and increasing ocean alkalinity by ~10% throughout the water column (Fig. 4 *B* and *C*). This large change in the CCD is inconsistent with available data (20, 24) and the previously tuned model (ref. 16, and references therein), suggesting that other carbon cycle model parameters need to be reassessed. We were then able to reproduce the measured CCD and alkalinity values by varying one poorly constrained geological variable—the riverine alkalinity flux (Fig. 4 *B* and *C*) (13, 25). Tuning for either the CCD or deep ocean alkalinity resulted in a riverine alkalinity flux that is lower than the estimated present-day value of 12×10^{12} molC/y (20, 26) or the Early Paleogene value of ~15.8×10^{12} molC/y (16) previously tuned by LOSCAR with an outdated bathymetry reconstruction. The obtained value (6.2 to 7.6×10^{12} molC/y) is consistent with recent surface process modeling estimates (27). While we have not exhaustively explored the Early Paleogene Earth system parameter space considering other model parameters (e.g., ocean mixing and ocean productivity), the strong sensitivity of riverine flux to bathymetric changes clearly illustrates that model calibrations must account for the bathymetry effect (mean depth and crucially distribution). Consider a gedanken experiment where we are trying to estimate the temporal evolution of global carbonate-silicate weathering fluxes by fitting CCD observations from ocean core data. The CCD is sensitive to weathering fluxes since reduced bicarbonate riverine flux limits ocean bicarbonate concentration, therefore, reducing ocean alkalinity, calcite saturation, ocean C sequestration, and shoaling the CCD. However, our results show that ocean bathymetry is another previously ignored strong sensitivity parameter to the CCD. Since ocean bathymetry is, to first order, reconstructable via standard geodynamical methods, it is a critical climate forcing that must be correctly accounted for.

Discussion

Our analysis clearly illustrates that the bathymetric effect—both mean depth and bathymetry distribution—on the C cycle is significant. Considering the plausible range of bathymetric configurations over the last 80 Myr of Earth's history, it cannot be ignored when studying the carbon cycle and inferring changes in ocean chemistry and productivity. Remarkably, up to 50% of the carbon cycle evolution throughout the Cenozoic can potentially be explained through bathymetry evolution alone. This evolution is important for describing the carbonate reservoir distribution, ocean alkalinity, and therefore the buffering capacity of the oceans. These effects are purely bathymetry driven, prescribing no change in ocean salinity or temperature yet producing similar trends in DIC and ocean alkalinity.

More broadly, the results highlight the importance of thinking about the long-term C cycle from the perspective of marine carbonate precipitation, dissolution, and deposition rather than just a balance between sources and sinks. Why is this the case? Because the ocean needs to reach saturation in a reasonable fraction of the oceans to deposit carbonates (C removal) and balance volcanic flux. If there is a significant amount of shallow shelf areas with ocean productivity, deposition can occur with a lower ocean alkalinity. Else, carbonate saturation in deeper ocean basins is needed for carbonate deposition, requiring a higher ocean alkalinity. Conceptually, the net impact of changing bathymetry is similar to the classic carbonate compensation feedback due to changes in ocean alkalinity following changes in ocean temperature, salinity, or productivity (23). Here, the captured C cycle feedback is driven by seafloor bathymetry changes and is thus especially relevant for long timescales. Since the ocean-dissolved carbon is the dominant C reservoir in the ocean-atmosphere system, changes in ocean carbonate chemistry directly influence the atmospheric C values on timescales of 10 s of kyr. On longer timescales (100 s of kyr), changes to atmospheric C (e.g., arising from tectonic evolution) are accommodated by silicate weathering feedbacks. Bathymetry evolution further informs changes in C cycles processes across multiple timescales through other feedbacks. For instance, changes

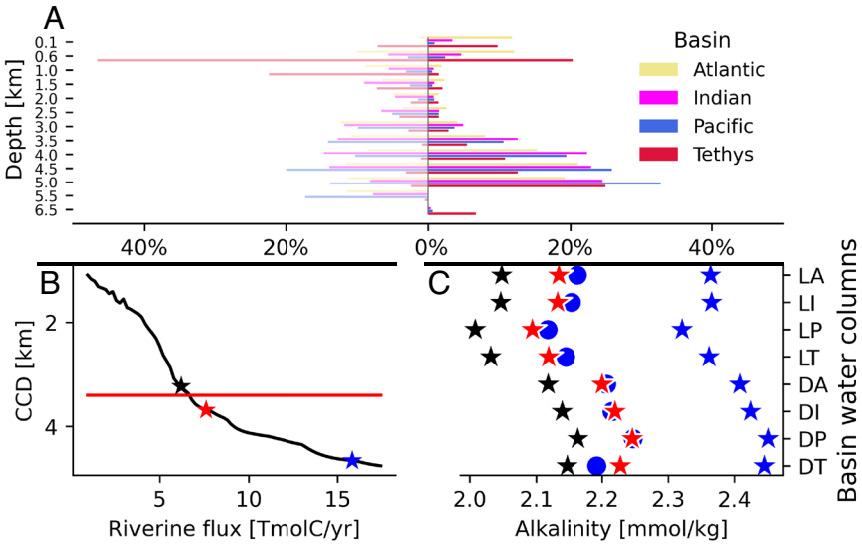

Fig. 4. Discrepancy of bathymetry influenced CCD as a function of riverine flux and ocean alkalinity. (*A*) Default LOSCAR bathymetry model (*Left*) and updated 60 Ma bathymetry reconstruction (*Right*). Perturbed steady-state CCD and ocean alkalinity using our updated bathymetry model and a shelf-deep marine sediment partition coefficient half its default LOSCAR value (FSHLF = 2.25). (*B*) Global CCD with updated bathymetry and varying the degree of initial $CaCO_3$ riverine flux. Blue, red, and black stars represent initial riverine fluxes corresponding to the default LOSCAR values, LOSCAR model CCD reproduction, and calibrated LOSCAR model alkalinity reproduction. The red line is a sediment core-derived global CCD with no specific riverine flux [Lyle et al. (24)]. (*C*) Corresponding ocean alkalinity throughout basin water columns (*SI Appendix*, Fig. S1) with the addition of LT and DT denoting the Tethys Ocean. The symbols as in *B* except for blue dots showing LOSCAR's default alkalinity.

in mid-ocean ridge spreading rate vary CO_2 outgassing and long-term weathering trends (100 s of kyr). Additionally, eustatic sea-level change due to bathymetric evolution (1 to 10 s of Myr) can lead to continental flooding, potentially increasing seafloor biomass, CO_2 from respiration, and dissolution of seafloor $CaCO_3$ sediment within calcite over-saturated bottom waters (28) on shorter timescales ranging 10 s of y to 100 s of kyr (ref. 29, and references therein). The strength of these influences is partially dependent on the spatio-temporal pattern of bathymetry changes and can be either net positive or negative feedbacks. Furthermore, a deposition-focused perspective illustrates that the distribution of sediment (partly bathymetry controlled) determines the ocean buffering capacity (through carbonate dissolution) to external CO_2 perturbations and how the system evolves/relaxes back to equilibrium. Finally, the sediment and seafloor carbonate deposition and subduction closes the long-term surface-interior C cycle loop. In other words, bathymetry is not just a boundary condition (let alone constant!). It is also the driver of change, controlling depositional areas, consumption of riverine flux, and the chemical state of individual ocean basins. Seafloor bathymetry truly represents the interface along which the solid earth and ocean lie and actively interact.

While our reconstructions are restricted to the past 80 Myr, large variations to bathymetry can be inferred from reconstructed seafloor ages throughout the last 230 Myr (30) and even back to 410 Ma when approximating seafloor age from past plate configurations (31). From a climate modeling perspective, future reconstructions will benefit from careful modeling of processes affecting shallow (0 to 600 m), intermediate (600 to ~2,500 m), and deep (>2,500 m) bathymetry evolution not associated with the classical oceanic plate evolution: syn-rift extension and sediment deposition, continental shelf extent, mantle flow supported bathymetry (e.g., the Western Interior Seaway), seafloor volcanism (e.g., LIP, seamounts, and paleo island arcs), and glacier eustasy (32–34). Our model results highlight that the shallow bathymetry component leads to large CCD shifts. Despite the various challenges in reconstructing shallow seafloor area, we have identified it as high priority direction for future work and strongly recommend that geochemical models calibrate poorly constrained Earth system parameters (e.g., weathering rates, riverine flux to deep marine, conveyor transport, biological pump misinterpretation of productivity, and ocean chemistry are clearly illustrated by our Early Paleogene case study) while using period-appropriate bathymetry.

Although the focus of this study is the chemical processes associated with ocean bathymetry, chemical and physical processes are also coupled, through the interior-driven bathymetry evolution shaping Earth's biological ecosystem (e.g., productivity) and the long-term carbon cycle. The combination of gateways, continental shelves, magmatic emplacements, island arcs, and instances of seafloor roughness inform bathymetry evolution that can influence mixing rates, upwelling deep water nutrients, and therefore the spatial distribution and amount of biological production in surface waters (35). Changes in continental-ocean configuration directly affect the amount of riverine flux associated nutrients and alkalinity consumed in the shelves and unable to reach the deeper part of ocean basins. There is a rich set of coupled chemical–physical ocean dynamics feedbacks associated with changes in seafloor bathymetry driven by Earth's deep interior. Our results highlight that these should be studied as first-order effects to develop a better understanding of Earth's carbon cycle evolution and when comparing to the geological record at global and especially regional scales.

Some of these bathymetry-associated couplings become increasingly important for the Early Cretaceous with the advent of calcareous phytoplankton (ref. 36, and references therein) and significant change in the ratio of deep ocean vs shallow water sediments as global carbon sinks (14). On Earth today, about half of the global carbonate burial occurs at shallow depths (< 200 m water depth) on continental shelves (Neritic carbonate) while the rest occurs on the deeper ocean floor (above the CCD). Prior to ~250 Ma, carbonate precipitation in Earth's oceans was caused only by neritic organisms such as corals (37), and carbonates were deposited only in shallow shelf regions. Furthermore, the Early Cretaceous exhibits a rich diversity of tectonic events: the formation and destruction of carbonate depositional zones with the formation of the south Atlantic basin, continued breakoff of Greater India from Gondwana, and emplacement of large-scale continental and oceanic flood basalts. These lead to strong variations in ocean circulation patterns, mixing rates, and the spatial pattern of upwelling zones (associated with high productivity). Previously, the carbon cycle has been shown to have a strong dependence on such changes in ocean circulation and mixing (ref. 9, and references therein) since the ocean is the main C reservoir. Here, we showed bathymetry also independently modulates the long-term carbon cycle's chemical processes. Therefore, the long-term C cycle on Earth is better understood when evolving bathymetry is self-consistently coupled with chemical processes and ocean dynamics changes.

The significant coupling between the evolution of the carbon sequestration depth and seafloor evolution suggests that the vast differences in seafloor age distributions spanning the last 410 Myr (31, 38) will affect global bathymetry, the depth of carbon sequestration, and therefore carbon cycling to the solid Earth and the subsequent rates of volcanic outgassing from subduction zones and mid-ocean ridges. Mid-ocean ridges, island arcs, and oceanic plateau formation contribute to bathymetry evolution, are non-unique to the recent past, or even Earth, and could be statistically constrained (32, 39) where direct reconstruction methods are inapplicable. Since the planetary bathymetry distribution is controlled by the planet's interior geodynamics and tectonics, the bathymetric influence on carbon cycling represents another important coupling between the solid planet and its surface–atmosphere environment. While present models analyzing the habitability of Earth and Earth-like planets to remain habitable have extensively focused on the role of continental and seafloor silicate weathering, the role of bathymetry-controlled carbonate deposition in modulating atmospheric CO_2 remains unstudied (40). Given the large diversity in geodynamics and ocean volumes for terrestrial exoplanets, analysis of bathymetry-associated effects will provide different constraints on planetary habitability and how it evolves following a large internal (e.g., volcanic eruption) or external (e.g., orbital forcings) perturbation.

Materials and Methods

Bathymetry Reconstructions. Bathymetry reconstructions were assembled over the last 80 Myr, consisting of the major evolving deep and shallow marine components. Similar to previous bathymetry reconstructions (15), we use the age–depth relationship of Crosby and McKenzie (4, 18) to convert the age of the oceanic lithosphere from paleoisochrons to compute the thermal evolution and subsidence of the oceanic lithosphere. These reconstructions were further modified by adding isostatically compensated global paleodeep marine sediment distributions using a relationship based on present-day sediment thickness and ocean crust age (41, 42). Continental shelves, flooded continental crust, and deep marine not represented in the plate motion model reconstructions were supplemented by paleo digital elevation maps (43). Bathymetry was then corrected for eustatic sea-level using the long-term Haq87 sea level curve (44), which is broadly consistent with paleoDEMs shoreline reconstructions. The evolved global bathymetry distributions were deformed based on present-day model uncertainty to reproduce accurate global ocean container volumes throughout the reconstruction period (*SI Appendix*, Fig. S12).

In consideration of reconstruction complexities and covarying shallow and deep bathymetry, we also produced a set of synthetic bathymetry models to compare with reconstructions. These consist of a roughly Gaussian type distribution (σ = 500 m) of deep bathymetry and varying uniform shallow bathymetry ($\leq$600 m) areal extents within realistic ranges predicted over the reconstruction period. Synthetic bathymetry has no basin distribution uniqueness (i.e., same depths in each basin) in contrast to geologic reconstructions.

C Cycle Modeling. The bathymetric effect on the carbon cycle was evaluated by a narrowly modified Earth system model: long-term ocean–atmosphere-sediment carbon cycle reservoir (LOSCAR). LOSCAR models ocean–atmospheric chemistry through ocean circulation, mixing, air–sea gas exchange, degassing, weathering, and a biological pump within a box model representing the atmosphere, a high latitude ocean, and ocean basins with 3 water column boxes (*SI Appendix*, Methods A). Since LOSCAR and variants have been used in numerous studies for the evaluation of paleo climates (13, 20, 45, 46), we use it to examine the influences of bathymetric components on ocean chemistry. We expect broadly similar behavior in other intermediate complexity ESMs, namely GEOCARBSULF variants (47), COPSE (48), GEOCLIM (10), and DCESS (49).

The default present-day LOSCAR model setup, parameterizing the Atlantic, Indian, and Pacific oceans, was used to calculate our synthetic and evolving bathymetry steady-state parameters (Figs. 2 and 3). Since LOSCAR describes ~500 m sediment box intervals from 100 m to 6,500 m, we parameterize our bathymetry distributions likewise for accurate comparison with the existing present-day LOSCAR bathymetry and associated parameter calibrations. Ocean floor area and volume were also evolved in LOSCAR with each reconstruction (*SI Appendix*, Methods B). The area of the high-latitude box represents cold surface waters globally, not purely high-latitude ocean floor. However, for simplicity, we describe the high-latitude bathymetry as the 10% (by area) of ocean floor at the highest latitudes following the original LOSCAR setup. For the majority of our calculations, we turned off calcite and silicate weathering feedbacks to determine the steady state determined primarily by ocean carbonate chemistry without coupled pCO_2–weathering flux changes.

The default Paleo LOSCAR model setup, parameterizing the present-day and Tethys oceans as four ocean basin boxes, was used to calculate 60 Ma bathymetry steady-state parameters (Fig. 4). The model setup is the same as described for synthetic and evolving bathymetry runs except the silicate and carbonate weathering feedbacks are included and riverine shelf partitioning is reduced by 50%. We impose the riverine shelf partitioning condition to stabilize the Earth system model.

Data, Materials, and Software Availability. The source codes, models, and Jupyter notebooks for reproducing figures and results in this paper are available at https://doi.org/10.5281/zenodo.10460278 (50).

ACKNOWLEDGMENTS. We would like to thank Richard Zeebe for providing the Earth System model code, LOSCAR. This project is supported by the NSF under grant EAR-1900633 to C.L.-B. C.L.-B. was also supported by the Louis B. and Martha B. Slichter Endowed Chair in Geosciences fund.

1. H. C. Urey, On the early chemical history of the earth and the origin of life. *Proc. Natl. Acad. Sci. U.S.A.* **38**, 351–363 (1952).
2. F. J. Millero, Thermodynamics of the carbon dioxide system in the oceans. *Geochim. Cosmochim. Acta* **59**, 661–677 (1995).
3. R. D. Müller *et al.*, A tectonic-rules-based mantle reference frame since 1 billion years ago–Implications for supercontinent cycles and plate–mantle system evolution. *Solid Earth* **13**, 1127–1159 (2022).
4. R. D. Müller *et al.*, A global plate model including lithospheric deformation along major rifts and orogens since the Triassic. *Tectonics* **38**, 1884–1907 (2019).
5. R. D. Müller, M. Sdrolias, C. Gaina, W. R. Roest, Age, spreading rates, and spreading asymmetry of the world's ocean crust. *Geochem. Geophy. Geosyst.* **9**, Q04006 (2008).
6. D. C. Engebretson, A. Cox, R. G. Gordon, Relative motions between oceanic and continental plates in the Pacific Basin/David C. Engebretson, Allan Cox, Richard G. Gordon, Special paper/Geological Society of America; 206 (Geological Society of America, Boulder, Colo, 1985).
7. J.-B. Ladant *et al.*, Paleogeographic controls on the evolution of Late Cretaceous ocean circulation. *Clim. Past* **16**, 973–1006 (2020).
8. E. O. Straume, C. Gaina, S. Medvedev, K. H. Nisancioglu, Global Cenozoic paleobathymetry with a focus on the Northern Hemisphere oceanic gateways. *Gondwana Res.* **86**, 126–143 (2020).
9. N. Herold *et al.*, A suite of early Eocene (~55 Ma) climate model boundary conditions. *Geosci. Model Dev.* **7**, 2077–2090 (2014).
10. Y. Donnadieu *et al.*, A GEOCLIM simulation of climatic and biogeochemical consequences of Pangea breakup. *Geochem. Geophys. Geosyst.* **7**, Q11019 (2006).
11. W. H. Berger, Increase of carbon dioxide in the atmosphere during deglaciation: The coral reef hypothesis. *Naturwissenschaften* **69**, 87–88 (1982).
12. E. C. Geyman *et al.*, The origin of carbonate mud and implications for global climate. *Proc. Natl. Acad. Sci. U.S.A.* **119**, e2210617119 (2022).
13. N. Komar, R. E. Zeebe, Reconciling atmospheric CO2, weathering, and calcite compensation depth across the Cenozoic. *Sci. Adv.* **7**, eabd4876 (2021).
14. R. D. Müller *et al.*, Evolution of Earth's tectonic carbon conveyor belt. *Nature* **605**, 629–639 (2022).
15. A. Dutkiewicz, R. D. Müller, J. Cannon, S. Vaughan, S. Zahirovic, Sequestration and subduction of deep-sea carbonate in the global ocean since the Early Cretaceous. *Geology* **47**, 91–94 (2018).
16. R. E. Zeebe, LOSCAR: Long-term Ocean-atmosphere-Sediment CArbon cycle Reservoir Model v2.0.4. *Geosci. Model Dev.* **5**, 149–166 (2012).
17. A. Ridgwell, Interpreting transient carbonate compensation depth changes by marine sediment core modeling. *Paleoceanography* **22**, PA4102 (2007).
18. A. G. Crosby, D. McKenzie, An analysis of young ocean depth, gravity and global residual topography. *Geophys. J. Int.* **178**, 1198–1219 (2009).
19. J. J. Middelburg, K. Soetaert, M. Hagens, Ocean Alkalinity, Buffering and biogeochemical processes. *Rev. Geophys.* **58**, e2019RG000681 (2020).
20. H. Pälike *et al.*, A Cenozoic record of the equatorial Pacific carbonate compensation depth. *Nature* **488**, 609–614 (2012).
21. D. M. Sigman, E. A. Boyle, Glacial/interglacial variations in atmospheric carbon dioxide. *Nature* **407**, 859–869 (2000).
22. C. T. Hayes *et al.*, Global ocean sediment composition and burial flux in the deep sea. *Global Biogeochem. Cycles* **35**, e2020GB006769 (2021).
23. D. A. Siegel, T. DeVries, I. Cetinić, K. M. Bisson, Quantifying the Ocean's biological pump and its carbon cycle impacts on global scales. *Annu. Rev. Marine Sci.* **15**, 329–356 (2023).
24. M. Lyle *et al.*, Pacific Ocean and Cenozoic evolution of climate. *Rev. Geophys.* **46**, RG2002 (2008).
25. R. van der Ploeg, B. P. Boudreau, J. J. Middelburg, A. Sluijs, Cenozoic carbonate burial along continental margins. *Geology* **47**, 1025–1028 (2019).
26. J. W. Morse, F. T. Mackenzie, Geochemistry of sedimentary carbonates/John W. Morse, Fred T. Mackenzie, Developments in sedimentology (Elsevier, Amsterdam, 1990), vol. 48.
27. T. Salles, L. Husson, M. Lorcery, B. Hadler Boggiani, Landscape dynamics and the Phanerozoic diversification of the biosphere. *Nature* **624**, 115–121 (2023).
28. D. E. Archer, An atlas of the distribution of calcium carbonate in sediments of the deep sea. *Global Biogeochem. Cycles* **10**, 159–174 (1996).
29. M. R. Raven *et al.*, Biomass storage in anoxic marine basins: Initial estimates of geochemical impacts and CO2 sequestration capacity. *AGU Adv.* **5**, e2023AV000950 (2024).
30. R. D. Müller *et al.*, Ocean basin evolution and global-scale plate reorganization events since Pangea Breakup. *Annu. Rev. Earth Planet. Sci.* **44**, 107–138 (2016).
31. S. Williams, N. M. Wright, J. Cannon, N. Flament, R. D. Müller, Reconstructing seafloor age distributions in lost ocean basins. *Geosci. Front.* **12**, 769–780 (2021).
32. A. Goswami, L. Hinnov, A. Gnanadesikan, T. Young, Realistic paleobathymetry of the cenomanian-turonian (94 Ma) boundary global ocean. *Geosciences* **8**, 21 (2018).
33. A. M. Forte, D. B. Rowley, Earth's isostatic and dynamic topography–A critical perspective. *Geochem. Geophys. Geosyst.* **23**, e2021GC009740 (2022).
34. A. Young *et al.*, Long-term Phanerozoic sea level change from solid Earth processes. *Earth Planet. Sci. Lett.* **584**, 117451 (2022).
35. K. L. Polzin, J. M. Toole, J. R. Ledwell, R. W. Schmitt, Spatial variability of turbulent mixing in the Abyssal Ocean. *Science* **276**, 93–96 (1997).
36. S. Rigby, C. V. Milsom, Origins, evolution, and diversification of zooplankton. *Annu. Rev. Ecol. Systemat.* **31**, 293–313 (2000).
37. R. E. Martin, Cyclic and secular variation in microfossil biomineralization: Clues to the biogeochemical evolution of Phanerozoic oceans. *Global Planet. Change* **11**, 1–23 (1995).
38. R. D. Müller, M. Seton, "Paleophysiography of Ocean Basins" in *Encyclopedia of Marine Geosciences*, J. Harff, M. Meschede, S. Petersen, J. Thiede, Eds. (Springer Netherlands, Dordrecht, 2014), pp. 1–15.
39. E. Cañón-Tapia, Seamount chains and hotspot tracks: Superficially similar, deeply different. *Geosci. Front.* **14**, 101659 (2023).
40. O. R. Lehmer, D. C. Catling, J. Krissansen-Totton, Carbonate-silicate cycle predictions of Earth-like planetary climates and testing the habitable zone concept. *Nat. Commun.* **11**, 6153 (2020).
41. E. O. Straume *et al.*, GlobSed: Updated total sediment thickness in the World's Oceans. *Geochem. Geophys. Geosyst.* **20**, 1756–1772 (2019).
42. M. J. Hoggard, J. Winterbourne, K. Czarnota, N. White, Oceanic residual depth measurements, the plate cooling model, and global dynamic topography. *J. Geophys. Res. Solid Earth* **122**, 2328–2372 (2017).
43. C. R. Scotese, N. M. Wright, PALEOMAP Paleodigital Elevation Models (PaleoDEMS) for the Phanerozoic. Zenodo. https://doi.org/10.5281/zenodo.5460860. Deposited 11 November 2021.
44. B. U. Haq, J. A. N. Hardenbol, P. R. Vail, Chronology of fluctuating sea levels since the Triassic. *Science* **235**, 1156–1167 (1987).
45. T. H. Heimdal, M. T. Jones, H. H. Svensen, Thermogenic carbon release from the Central Atlantic magmatic province caused major end-Triassic carbon cycle perturbations. *Proc. Natl. Acad. Sci. U.S.A.* **117**, 11968–11974 (2020).
46. R. E. Zeebe, A. Ridgwell, J. C. Zachos, Anthropogenic carbon release rate unprecedented during the past 66 million years. *Nat. Geosci.* **9**, 325–329 (2016).
47. A. B. Robert, GEOCARBSULF: A combined model for Phanerozoic atmospheric O2 and CO2. *Geochim. Cosmochim. Acta* **70**, 5653–5664 (2006).
48. T. M. Lenton, S. J. Daines, B. J. W. Mills, COPSE reloaded: An improved model of biogeochemical cycling over Phanerozoic time. *Earth Sci. Rev.* **178**, 1–28 (2018).
49. G. Shaffer *et al.*, Implementation of methane cycling for deep-time global warming simulations with the DCESS Earth system model (version 1.2). *Geosci. Model Dev.* **10**, 4081–4103 (2017).
50. M. Bogumil, T. Mittal, C. Lithgow-Bertelloni, The effects of bathymetry on the CCD: Implications for the long-term carbon cycle. Zenodo. https://doi.org/10.5281/zenodo.10460278. Deposited 5 January 2024.